Structure of the hard ellipsoid fluid

J. Talbot[a] and D. Kivelson
Department of Chemistry and Biochemistry, University of California at Los Angeles, Los Angeles, California 90024

M. P. Allen
H. H. Wills Physics Laboratory, University of Bristol, Bristol BS8 1TL, England

G. T. Evans
Department of Chemistry, Oregon State University, Corvallis, Oregon 97331

D. Frenkel
FOM-Institute for Atomic and Molecular Physics, P. O. Box 41883, 1009 DB Amsterdam, The Netherlands

(Received 26 June 1989; accepted 1 November 1989)

Molecular-dynamics calculations are reported on fluids of hard ellipsoids over a range of densities and for several ellipsoidal aspect ratios. The pair correlation functions obtained from the simulations are expressed as functions of the minimum surface-to-surface separation, s, measured along the surface normal, $\hat{\mathbf{s}}$, and angles measured relative to the surface normal. Both isotropic and orientational correlations exhibit simpler behavior in the surface-to-surface than in the more customary center-to-center coordinate representation. For the hard-ellipsoid fluid, the isotropic part of the pair correlation function, $g_{\rm iso}(s)$, behaves much like that of a hard-sphere fluid. The surface-to-surface coordinates are well suited for studying pressure and collision rates because these properties depend upon surface contact distributions. They are also useful for studying the orientational order parameter, g_2, because they enable one to readily identify a long-range part and geometrical excluded volume contribution.

INTRODUCTION

The hard-sphere fluid has proved to be an excellent model for atomic fluids because fluid structure is determined largely by short-range repulsive interactions. Long-range interactions can be regarded as perturbations, and various theories based on appropriate hard-sphere reference states have been developed that allow the systematic inclusion of potential softness.[1,2]

Molecular fluids are much more difficult to treat theoretically. Although the same physical principals should apply (structure being largely determined by repulsive interactions), it is no longer obvious what the hard-core reference fluid should be. In the interaction site model[3,4] the reference fluid is a system of fused hard spheres (e.g., dumbbells). Alternatively, one can choose a hard convex body (HCB) representation of the core of a molecule.[5] There are a number of advantages in using the HCB: analytical calculations of some aspects of the pair distribution function[6,7] (PDF) and of a few transport properties[8] are feasible and have been accomplished. Until recently,[9,10] the application and adoption of the HCB approach has been hindered by the paucity of simulation data. Existing theory could not be tested fully, and it was unclear if the HCB model would prove to be as valuable as the hard-sphere model as a reference fluid for real fluids with soft potentials.

The present goal is to provide additional simulation data on the HCB system with particular emphasis on the properties of the expansion of the PDF in terms of complete sets of angular functions. Common expressions of the PDF for a polyatomic fluid of $D_{\infty h}$ molecules require the specification of the center-to-center separation, r, and three angles.[4,11,12] The primary purpose of this paper is to explore an alternative choice of variables based on the surface-to-surface distance s, and to discuss the PDF and various physical quantities derivable from the PDF. In particular, we focus on the hard-ellipsoid fluid.

THEORY

Representation of the pair distribution function (PDF)

The conventional coordinates of a fluid of $D_{\infty h}$ molecules are the center-to-center vector $\mathbf{r}$ and the orientation vectors $\hat{\mathbf{e}}_1$ and $\hat{\mathbf{e}}_2$, of the two molecules. Of these seven coordinates three are superfluous and only four are required to specify the mutual orientation of two molecules in an isotropic fluid. These four coordinates are usually taken to be the center-to-center distance, the polar angles $\arccos(\hat{\mathbf{e}}_1\cdot\hat{\mathbf{r}})$ and $\arccos(\hat{\mathbf{e}}_2\cdot\hat{\mathbf{r}})$, and $\phi_1-\phi_2$, where ϕ_1 and ϕ_2 are the azimuthal angles of $\hat{\mathbf{e}}_1$ and $\hat{\mathbf{e}}_2$ with respect to $\hat{\mathbf{r}}$. The spherical harmonic expansion of the PDF based on these variables is[11,12]

$$g(r,\hat{\mathbf{e}}_1,\hat{\mathbf{e}}_2)=\sum g_{ll'm}(r)C_{lm}(\hat{\mathbf{e}}_1)C^*_{l'm}(\hat{\mathbf{e}}_2)\,, \qquad (1)$$

where the C_{lm}'s are modified spherical harmonics. Equation (1) has become a cornerstone in the analysis of stuctural properties of polyatomic fluids. The most troublesome property of Eq. (1) is that it represents orientational correlations on spherical surfaces. In the isotropic phase and at large

[a] Present address: School of Chemical Engineering, Purdue University, West Lafayette, IN 47907.

 0021-9606/90/053048-10$03.00

intermolecular separations, orientational correlations are nearly isotropic and the PDF can be expressed succinctly with a few terms in the expansion. However, for molecules in close proximity, where steric correlations are strong, the local symmetry is not spherical, and as a result Eq. (1) has poor convergence properties.[13]

In response to these well-documented shortcomings of the conventional expansions of the PDF, Kabadi and Steele[14] suggested that for soft nonspherical bodies the variables in the PDF should be based upon the properties of the equipotentials. Their chosen angular coordinates where identical to those used above, but their distance variable was taken as the center-to-center distance scaled by the angle-dependent Lennard–Jones diameter. In contrast to calculations based on Eq. (1), by means of this approach, the thermodynamic properties are easily obtained and the spherical harmonic expansion is rapidly convergent. For systems of HCB's we can replace the equipotentials by the hard-core surface.

For a fluid of HCB's Kumar, James, and Evans[15] proposed an expansion in which the pair correlation function (PCF) is expressed as a function of the surface-to-surface distance s and three angles (θ_1, θ_2 and α) measured with respect to the normal $\hat{\mathbf{s}}$ or apse vector specifying the minimum surface-to-surface distance. See Fig. 1. These coordinates are defined by

$$\cos\theta_n = \hat{\mathbf{s}}\cdot\hat{\mathbf{e}}_n \equiv x_n \quad \text{for } n = 1,2 \tag{2}$$

with α the angle between the plane defined by $(\hat{\mathbf{e}}_1,\hat{\mathbf{s}})$ and $(\hat{\mathbf{e}}_2,\hat{\mathbf{s}})$. The Jacobian J for this transformation from center-to-center coordinates to the surface-to-surface coordinates is a function of s and the new angles (see Appendix A).

In this new language, one could in principal expand the PCF in a set of functions orthogonal in space with the Jacobian, $J(s,\hat{\mathbf{e}}_1,\hat{\mathbf{e}}_2)$. She, James and Evans[7(b)] did this by means of a separate Gram–Schmidt procedure at each value of s,

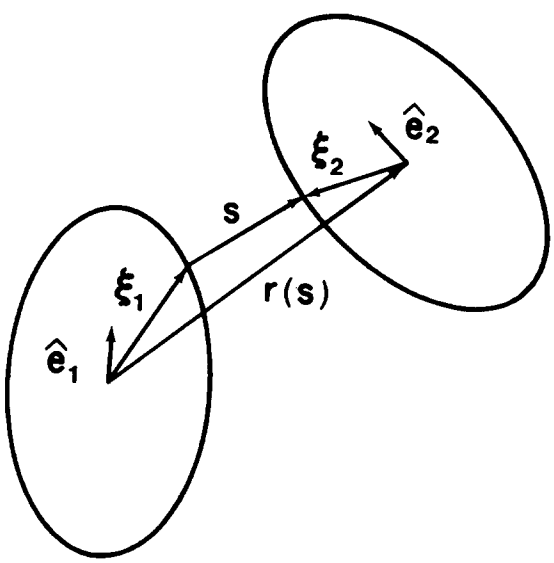

FIG. 1. The apse-vector-based coordinate system for two ellipsoids. The orientations $\hat{\mathbf{e}}_1$ and $\hat{\mathbf{e}}_2$ are measured with respect to the minimum surface-to-surface vector s. Each ellipsoid has a semimajor axis, a, and semiminor axis, b.

but this approach is cumbersome, and to circumvent these difficulties Kumar, James, and Evans[15] followed a procedure proposed by Kabadi and Steele[14] in which the product of g and J are expanded in spherical harmonics. Thus, if

$$G(s,\hat{\mathbf{e}}_1,\hat{\mathbf{e}}_2) \equiv g(s,\hat{\mathbf{e}}_1,\hat{\mathbf{e}}_2)J(s,\hat{\mathbf{e}}_1,\hat{\mathbf{e}}_2), \tag{3}$$

then

$$G(s,\hat{\mathbf{e}}_1,\hat{\mathbf{e}}_2) = \sum G_{ll'm}(s)C_{lm}(\hat{\mathbf{e}}_1)C^*_{l'm}(\hat{\mathbf{e}}_2), \tag{4}$$

where $\hat{\mathbf{e}}_1$ and $\hat{\mathbf{e}}_2$ are expressed with respect to $\hat{\mathbf{s}}$ rather than $\hat{\mathbf{r}}$. The advantage to this approach is that the contact surface is represented by the $s = 0$ value. The distribution function $G(s,\hat{\mathbf{e}}_1,\hat{\mathbf{e}}_2)$ reflects the anisotropy of the Jacobian $J(s,\hat{\mathbf{e}}_1,\hat{\mathbf{e}}_2)$ as well as the anisotropy introduced by actual molecular order. It is the latter which interests us, and in order to isolate these effects we consider an expansion of $J(s,\hat{\mathbf{e}}_2,\hat{\mathbf{e}}_2)$ similar to that described for G in Eq. (4),

$$J(s,\hat{\mathbf{e}}_1,\hat{\mathbf{e}}_2) = \sum J_{ll'm}(s)C_{lm}(\hat{\mathbf{e}}_1)C^*_{l'm}(\hat{\mathbf{e}}_2)\,. \tag{5}$$

Clearly, the choice of orientation angles and distances for g is not unique. For example, Ghazi and Rigby[16] investigated the structural properties of hard spherocylinder fluids using a spherical harmonic expansion of the PCF with an angle-dependent separation variable. In accord with Kabadi and Steele, they also find a simple and a weakly structured dependence of the expansion coefficients of g on separation and they find an isotropic component of g with behavior reminiscent of a hard-sphere fluid.

In the following section, we summarize the relationship of various thermodynamic and structural properties to G, the apse-vector-based PCF, and try to assess its utility.

ISOTROPIC PROPERTIES

We define the isotropic PDF, $g_{\rm iso}(s)$, as

$$S(s)g_{\rm iso}(s) = \int (d\hat{\mathbf{e}}_1/4\pi)\int (d\hat{\mathbf{e}}_2/4\pi)G(s,\hat{\mathbf{e}}_1,\hat{\mathbf{e}}_2), \tag{6}$$

where $4\pi S(s)$ is the surface area of the excluded volume defined by

$$S(s) = \int (d\hat{\mathbf{e}}_1/4\pi)\int (d\hat{\mathbf{e}}_2/4\pi)J(s,\hat{\mathbf{e}}_1,\hat{\mathbf{e}}_2). \tag{7}$$

$g_{\rm iso}(s)$ is an interesting quantity because in many ways it is analogous to the PDF for spheres in which $g_{000}(r)$ is integrated over r^2dr, while $g_{\rm iso}(s)$ is integrated over $S(s)ds$. Note that for hard spheres of diameter σ, the area $S(s) = (\sigma + s)^2$; for HCB's $S(s)$ was obtained by Kihara,[5] and is given in Appendix A.

It can readily be seen that

$$g_{\rm iso}(s) = G_{000}(s)/S(s), \tag{8}$$

which relates the isotropic PCF to the expansion coefficient, $G_{000}(s)$. Another method of obtaining the isotropic PDF is by counting the number of neigbors in shells of diameter s. If $N(s)$ is the number of neighbors inside the surface-to-surface distance s, then[15]

$$\frac{dN(s)}{ds} = 4\pi\rho G_{000}(s), \tag{9}$$

where ρ is the average number density. This relation can be used to evaluate $G_{000}(s)$, and with knowledge of $S(s)$ one can then use Eq. (8) to obtain $g_{\rm iso}(s)$.

CONTACT PROPERTIES

A number of properties depend on the contact ($s=0$) values of the $G_{ll'm}(s)$'s. For these properties it is convenient to define the average $\overline{A(s)}$ corresponding to a quantity $A(s,\hat{\mathbf{e}}_1,\hat{\mathbf{e}}_2)$:

$$\overline{A(s)} = \frac{\int (d\hat{\mathbf{e}}_1/4\pi) \int (d\hat{\mathbf{e}}_2/4\pi) GA}{G_{000}(s)}. \tag{10}$$

The contact average $\overline{A(s=0)}$ enters expressions for such physical quantities as pressure and collision rate, and can be directly calculated in a molecular-dynamics (MD) simulation by averaging A over all molecular contact pairs. The quantity $4\pi\rho S(s) g_{\rm iso}(s)\, \overline{A(s)} ds$ is the integral over all molecular orientations in a shell at a distance s, and $4\pi\rho S(s) g_{\rm iso}(s) ds$ is the number of molecules in that shell; thus $\overline{A(s)}$ is the average per molecule of A taken over molecules in a given shell. As a consequence, averages such as $\overline{A(s)}$ can be readily determined in a MD simulation. Note that the apse-vector representation is much more convenient for calculating contact properties than the center-to-center coordinate system where an infinite number of spherical harmonic coefficients are required.

Pressure

Boublik has derived an expression for the pressure of a monocomponent fluid of HCB's. In our notation his expression is[6]

$$\beta P/\rho = 1 + 4\pi(\rho/3) S(0) g_{\rm iso}(0)\, \overline{h(0)}, \tag{11}$$

where $\overline{h(s)}$ is the average of the support function $h(x_1)$ for the convex body.

The pressure can also be expressed in terms of the G expansion coefficients. Upon insertion of Eqs. (3) and (10) into Eq. (11), we find that

$$\beta P/\rho = 1 + (4\pi\rho b/3) \sum_{n=0}^{\infty} a_{2n} G_{2n,0,0}(0), \tag{12}$$

where

$$a_{2n} = \sqrt{4n+1} \int_0^1 [h(x)/b\,] P_{2n}(x) dx. \tag{13}$$

$P_{2n}(x)$ is a Legendre polynomial, and b is the semiminor axis of the HCB. Although no general analytic expression for the a_n coefficients is known, we give explicit expressions for the first three in Appendix A, and numerical values in Table I.

There are two alternative routes to the pressure: from Eq. (11) since $\overline{h(0)}$ is directly measurable in MD simulations, and from the virial theorem applied to hard-core particles. The latter method requires the computation of the average impulse over collisions:[17]

$$\beta P/\rho = 1 + \beta \sum_{\text{collisions}} \mathbf{I}_{ij} \cdot \mathbf{r}_{ij}/(3Nt), \tag{14}$$

where $\mathbf{I}_{ij}$ is the impulse of the collision between ellipsoids i and j, the center-to-center separation at collision is r_{ij}, and t is the time over which the dynamics are followed.

TABLE I. Values of $S(s=0)$ and the pressure expansion coefficients. See Eqs. (14), (A12), (A13), and (A8).

a/b	a_0	a_2	a_4	a_6	$S(0)/I^2$
2	1.380	0.307	−0.027	0.004	1.14
3	1.81	0.614	−0.080	0.21	1.38
5	2.734	1.215	−0.207	0.069	1.96

Collision rate

The collision rate Z for identical particles is also given by an integral over the excluded volume surface,

$$\begin{aligned} Z &= \tfrac{1}{2}\rho v_r \int d\hat{\mathbf{s}} \int (d\hat{\mathbf{e}}_1/4\pi) \int (d\hat{\mathbf{e}}_2/4\pi) \\ &\quad \times G(s=0,\hat{\mathbf{e}}_1,\hat{\mathbf{e}}_2) D(x_1,x_2) \\ &= 2\pi\rho v_r g_{\rm iso}(s=0) S(s=0) \bar{D}, \end{aligned} \tag{15}$$

where $\bar{D}$ is the average of the momentum transfer function, $D(x_1,x_2)$, defined by

$$\begin{aligned} D^2(x_1,x_2) &= 1 + (\mu/I)[h'(x_1)^2(1-x_1^2) \\ &\quad + h'(x_2)^2(1-x_2^2)] \end{aligned} \tag{16}$$

where primes denote differentiation with respect to the argument, I is the moment of inertia, v_r is the relative thermal speed $[(8k_BT/\pi\mu)^{1/2}]$, and μ is the reduced mass $m/2$ of the colliding pair. D can be determined directly in the simulation, as can Z; Eq. (15) therefore provides a route to $g_{\rm iso}(s=0)$. Values of $g_{\rm iso}(s=0)$, which must be equal to $G_{000}(s=0)/S(s=0)$ [see Eq. (8)] are listed in Table II.

ORIENTATIONAL PROPERTIES

The anisotropic expansion coefficients are angular averages of the "pair" orientational functions:

$$\begin{aligned} G_{ll'm}(s) &= \int (d\hat{\mathbf{e}}_1/4\pi) \int (d\hat{\mathbf{e}}_2/4\pi) G(s,\hat{\mathbf{e}}_1,\hat{\mathbf{e}}_2) \\ &\quad \times C_{lm}(\hat{\mathbf{e}}_1) C^*_{l'm}(\hat{\mathbf{e}}_2). \end{aligned} \tag{17}$$

TABLE II. MD contact values of $G_{n00}(s)/S(s)$ obtained by extrapolation of the distribution function. Values in parentheses were computed from the collision frequency Z and the MD value of $D(s=0)$; $\rho_0 = \sqrt{2}/I^3$.

a/b	ρ/ρ_0	$n=0$		$n=2$	$n=4$
2	0.5	3.45	(3.44)	−1.66	0.754
	0.6	4.83	(4.81)	−2.55	1.18
	0.7	7.21		−3.85	1.77
	0.8	11.52	(11.47)	−6.41	3.00
3	0.1	1.29		−0.75	0.47
	0.3	2.14	(2.03)	−1.34	0.82
	0.5	3.60	(3.64)	−2.53	1.63
	0.6	5.24	(5.10)	−3.83	2.49

These angular averages are of considerable interest since, for example, two often studied classes of orientational polynomials carrying packing information are the "single"-particle functions $C_{2m}(\hat{\mathbf{e}}_1)$ and the pair functions $C_{2m}(\hat{\mathbf{e}}_1)C^*_{2m}(\hat{\mathbf{e}}_2)$, which are related to $G_{200}(s)$ and $G_{22m}(s)$, respectively. Remember that these orientations are measured with respect to $\hat{\mathbf{s}}$, so that averages over $C_{2m}(\hat{\mathbf{e}}_1)$ do not necessarily vanish.

Light scattering g_2

An orientational parameter of interest, which is measured in depolarized light scattering experiments, is[18]

$$g_2 = 1 + \rho \int d\mathbf{r} \int (d\hat{\mathbf{e}}_1/4\pi) \times \int (d\hat{\mathbf{e}}_2/4\pi) P_2(\hat{\mathbf{e}}_1\cdot\hat{\mathbf{e}}_2) g(r,\hat{\mathbf{e}}_1,\hat{\mathbf{e}}_2), \tag{18}$$

where P_2 is the second-order Legendre polynomial. Equation (18) is expressed in center-to-center coordinates, but the radial integral converges rather slowly with increasing r, making it somewhat difficult to evaluate and rather difficult to interpret in terms of the positions and orientations of neighboring molecules.[19] We, therefore, wish to examine g_2 in apse-vector coordinates, but it is not straightforward to convert Eq. (18) to apse-vector coordinates. Difficulties arise because the triple integral in Eq. (18) is *conditionally* convergent. At large r the function $g(r,\hat{\mathbf{e}}_1,\hat{\mathbf{e}}_2) \to 1$, and the integrand of Eq. (18) approaches $P_2(\hat{\mathbf{e}}_1\cdot\hat{\mathbf{e}}_2)$, which has finite contributions at all values of r, and hence the integral over r diverges in the thermodynamic limit. The consequence of this is that one must first integrate over angles, in which case the integral vanishes for large values of r, and g_2 is therefore finite. Were the order of integration reversed, the integrations would yield an indeterminate quantity.

Since the transformation to apse-vector coordinates mixes $\mathbf{r}$, $\hat{\mathbf{e}}_1$, and $\hat{\mathbf{e}}_2$ [i.e., $\mathbf{s} = \mathbf{s}(\mathbf{r},\hat{\mathbf{e}}_1,\hat{\mathbf{e}}_2)$], we expect, and find, a divergent result when g_2 is reexpressed in the apse-vector coordinates. We can resolve this dilema by rearranging the integrand in Eq. (18) so as to make the integral absolutely convergent. This is done by rewriting g as $(g-1)+1$:

$$g_2 = 1 + \rho \int d\mathbf{r} \int \left(\frac{d\hat{\mathbf{e}}_1}{4\pi}\right) \times \int \left(\frac{d\hat{\mathbf{e}}_2}{4\pi}\right) P_2(\hat{\mathbf{e}}_1\cdot\hat{\mathbf{e}}_2)[g(r,\hat{\mathbf{e}}_1,\hat{\mathbf{e}}_2)-1] + \rho \int d\mathbf{r} \int \left(\frac{d\hat{\mathbf{e}}_1}{4\pi}\right) \int \left(\frac{d\hat{\mathbf{e}}_2}{4\pi}\right) P_2(\hat{\mathbf{e}}_1\cdot\hat{\mathbf{e}}_2). \tag{19}$$

The last term in Eq. (19) is zero, provided the angular integrations are carried out first. We divide the remaining integral into overlapping ($\mathscr{O}$) and non-overlapping ($\mathscr{NO}$) parts:

$$g_2 = 1 + \rho \int_{\mathscr{NO}} d\mathbf{r} \int \left(\frac{d\hat{\mathbf{e}}_1}{4\pi}\right) \times \int \left(\frac{d\hat{\mathbf{e}}_2}{4\pi}\right) P_2(\hat{\mathbf{e}}_1\cdot\hat{\mathbf{e}}_2)[g(r,\hat{\mathbf{e}}_1,\hat{\mathbf{e}}_2)-1] - \rho \int_{\mathscr{O}} d\mathbf{r} \int \left(\frac{d\hat{\mathbf{e}}_1}{4\pi}\right) \int \left(\frac{d\hat{\mathbf{e}}_2}{4\pi}\right) P_2(\hat{\mathbf{e}}_1\cdot\hat{\mathbf{e}}_2), \tag{20}$$

where we have used the fact that $g(r,\hat{\mathbf{e}}_1,\hat{\mathbf{e}}_2) = 0$ in the overlap region. We can transform the first integral of Eq. (20) to apse-vector coordinates because the integrand vanishes at large r, and this makes the integral absolutely convergent. The transformation replaces $d\mathbf{r}$ with $J\,d\mathbf{s}$ and gJ with G, so our final result for g_2 in the apse-vector system is

$$g_2 = 1 + \rho \int d\mathbf{s} \int \left(\frac{d\hat{\mathbf{e}}_1}{4\pi}\right) \times \int \left(\frac{d\hat{\mathbf{e}}_2}{4\pi}\right) [G(s,\hat{\mathbf{e}}_1,\hat{\mathbf{e}}_2) - J(s,\hat{\mathbf{e}}_1,\hat{\mathbf{e}}_2)] \times P_2(\hat{\mathbf{e}}_1\cdot\hat{\mathbf{e}}_2) - g_v, \tag{21}$$

where

$$g_v = \rho \int_{\mathscr{O}} d\mathbf{r} \int (d\hat{\mathbf{e}}_1/4\pi) \int (d\hat{\mathbf{e}}_2/4\pi) P_2(\hat{\mathbf{e}}_1\cdot\hat{\mathbf{e}}_2) \tag{22}$$

is a volume integral over the overlap region. Appendix B shows how to evaluate g_v by converting it to a surface integral:

$$g_v = 4\pi\rho \int (d\hat{\mathbf{e}}_1/4\pi) \int (d\hat{\mathbf{e}}_2/4\pi) \tfrac{1}{3} h_{12} \times J(0,\hat{\mathbf{e}}_1,\hat{\mathbf{e}}_2) P_2(\hat{\mathbf{e}}_1\cdot\hat{\mathbf{e}}_2). \tag{23}$$

with $h_{12} = h(x_1) + h(x_2)$. This completes the formal specification of g_2 in the apse-vector system.

SIMULATION

The equilibrium properties were obtained by analyzing configurations obtained from MD simulations of the hard-ellipsoid fluid. These simulations were performed in the microcanonical ensemble in a truncated octahedral cell.[20] The advantage of this geometry over the usual cubic cell is that it allows one to examine the correlations at greater distances for a given number of particles. This is particularly important with our present approach since the use of the surface-to-surface rather than center-to-center distance reduces the maximum range from a distance R_s to $R_s - 2a$, where R_s is the radius of the inscribing sphere of the simulation cell.

Two system sizes, $N = 125$ and $N = 512$, were employed. The unit of length used was l, where $l^3 = 8ab^2$ and a and b are the ellipsoid semimajor and semiminor axes, respectively. All the results reported here are for prolate ellipsoids of aspect ratios, $a/b = 2$ or 3, and for a density range $0.3 < \rho/\rho_0 < 0.8$, where

$$\rho_0 = \sqrt{2}/l^3 \tag{24}$$

is the density of closest packing. The runs were generally for a total of 10^6 collisions, and about 2000 configurations were saved at equal intervals for later analysis. Full details of the simulations are presented elsewhere.[21]

The minimum surface–surface distance determination is a nontrivial operation. Acceptable speed was obtained by use of a vectorized algorithm employing the curvature properties of the ellipsoids.[22]

RESULTS

Variation $g_{iso}(s)$ with s

There is considerable interest in finding spherical potentials which can be used to accurately model the properties of molecular fluids. In this connection we note that the $g_{iso}(s)$'s for 2:1 and 3:1 ellipsoids shown in Fig. 2 are similar to those for hard spheres (HS). We ask then if there is a reference HS fluid that can mimic this distribution function. An obvious choice is a HS fluid at the same density as the HCB fluid, where the hard spheres have the same volume as an ellipsoid: $\sigma^3 = 8ab^2$, where σ is the HS diameter. In Fig. 2 the distribution function of this HS fluid[23] is compared with the $g_{iso}(s)$ of the ellipsoid. The HS fluid has a second maximum around $s = \sigma$, whereas the second maximum in $g_{iso}(s)$ occurs over a range of s from $2a$ to $2b$. Because there are two length scales present in the HCB fluid, it appears impossible to find a HS fluid that has exactly the same surface-to-surface distribution function as the HCB. However, our chosen HS fluid accurately models the HCB fluid in the contact region (i.e., up to the second maximum).

Comparison of the apse-vector representation with conventional expansions

Figure 3(a) shows the spatial variation of the center-to-center isotropic PDF, $g_{000}(r)$, and its anisotropic expansion coefficients $g_{ll'm}(r)$. Even at the low density of $\rho/\rho_0 = 0.3$, both $g_{000}(r)$ and $g_{ll'm}(r)$ are highly structured. For comparison, in Fig. 3(b) we illustrate the s dependence of the expansion coefficients $G_{ll'm}(s)/S(s)$ for the same thermodynamic system; these ratios are taken as reasonable analogues of the $g_{ll'm}(r)$'s. A long-range tail is evident in

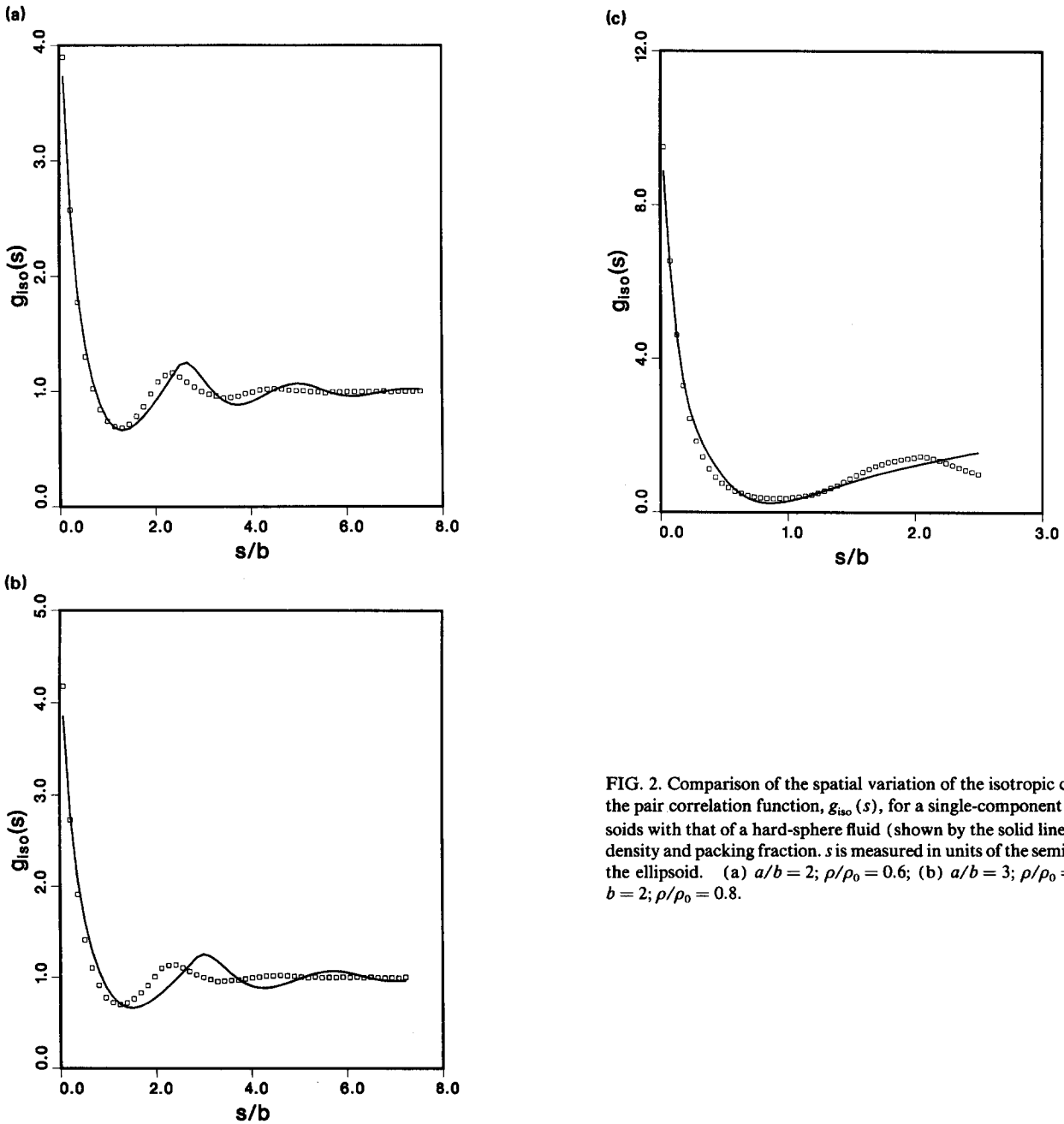

FIG. 2. Comparison of the spatial variation of the isotropic component of the pair correlation function, $g_{iso}(s)$, for a single-component fluid of ellipsoids with that of a hard-sphere fluid (shown by the solid line) at the same density and packing fraction. s is measured in units of the semiminor axis of the ellipsoid. (a) $a/b = 2$; $\rho/\rho_0 = 0.6$; (b) $a/b = 3$; $\rho/\rho_0 = 0.6$; (c) $a/b = 2$; $\rho/\rho_0 = 0.8$.

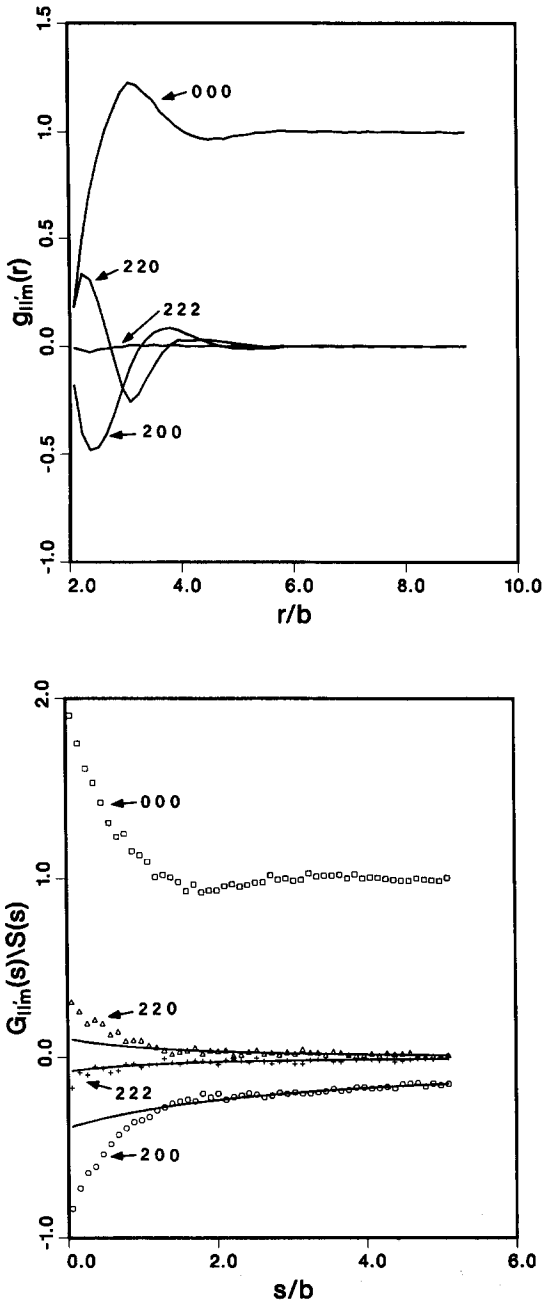

FIG. 3. Expansion coefficients for the hard-ellipsoid fluid with $a/b = 2$ and $\rho/\rho_0 = 0.3$. (a) In the center-to-center coordinate system: $g_{ll'm}(r)$ vs r/b. (b) In the apse-vector system: $G_{ll'm}(s)/S(s)$ and $J_{ll'm}(s)/S(s)$ vs s/b, given by broken and solid lines, respectively. (These simulations were for $N = 125$.)

$G_{ll'm}(s)/S(s)$, and this is explained by the orientational correlations contained in the Jacobian. The solid lines in Fig. 3(b) show the relaxing Jacobian, viz., $J_{ll'm}(s)/S(s)$. The true anisotropy in intermolecular packing is reflected in the difference between the solid lines and the data points, i.e., in the quantity $[G_{ll'm}(s) - J_{ll'm}(s)]/S(s)$ which enters as a component of Eq. (21). [Recall that $g_{ll'm}(r)$ starts at $r = 2b$, while $G_{ll'm}(s)$ starts at $s = 0$.]

Simple interpretation of the expansion coefficients, $G_{ll'm}(s)/S(s)$

The s dependence of a few $G_{ll'm}(s)/S(s)$ is shown in Fig. 3(b); these factors should be compared to the $g_{ll'm}(r)$'s in Fig. 3(a). In contrast to the $G_{ll'm}(s)$'s themselves, $G_{ll'm}(s)/S(s)$ are short range, decaying from the contact surface ($s = 0$), where they are localized and showing only small-amplitude oscillations which are density dependent.

Based upon the observed signs of the $G_{ll'm}(s)$ coefficients alone, one can get some idea of the structured environment around an ellipsoid. For example, the negative sign of $G_{200}(s)$ is consistent with $\langle P_2(\cos\theta_1)\rangle < 0$, and for this to be the case $\langle\theta_1\rangle > 54°$, where θ_1 is defined in Eq. (2). Similarly, the fact that $G_{400}(s)$ is positive suggests that $\langle\theta_1\rangle > 70°$. The magnitude of the 220 expansion coefficients are similar to the square root of the 200 terms, which suggests that the "pair" functions are only weakly correlated. With this information and a similar analysis of the 222 function, we are led to the conclusion that the out-of-plane angle, α, defined below Eq. (2), is in the range $45° < \alpha < 90°$. The picture that emerges from this qualitative analysis is that the molecules are aligned side by side with an out-of-plane angle greater than 45°. Generally, the 222 terms (which measure α correlations around 45°) are small, and for $a/b = 2$, at reduced density between 0.7 and 0.8, the 222 coefficients become more positive as the average angle between $\hat{\mathbf{e}}_1$ and $\hat{\mathbf{e}}_2$ diminishes.

Pressure

The determination of the pressure of a fluid of HCB's requires the use of the contact values of the PDF, see Eq. (12). Only a few of the apse-vector coefficients, $G_{2n,0,0}(0)$, are necessary in the computation of the pressure. To show this we present the results in Table III, where we show values of $(\beta P/\rho) - 1$ obtained by various truncations of Eq. (12). The sum is rapidly convergent because the a_{2n} coefficients decrease rapidly with n, as do the $G_{2n,0,0}(0)$: see Tables I and II. The values of $(\beta P/\rho) - 1$ calculated with only three

TABLE III. Convergence of the pressure expansion (calculated values of $\beta P/\rho - 1$).

		Number of terms[a]			
a/b	ρ/ρ_0[a]	One	Two	Three	Virial[b]
2	0.5	6.36	5.68	5.65	5.68
	0.6	10.70	9.44	9.39	9.47
	0.7	18.63	16.41	16.33	16.27
	0.8	34.04	29.83	29.65	29.60
3	0.1	0.66	0.53	0.52	0.50
	0.3	3.2	2.59	2.54	2.41
	0.5	9.24	7.04	6.85	7.01
	0.6	16.15	12.15	11.81	11.63

[a] The entries in Tables I and II were combined in Table III to determine the pressure by means of $\beta P/\rho - 1 = (2\pi/3)\sqrt{2}(b/a)^{1/3}(\rho/\rho_0)$ $S(0)\Sigma_n a_{2n}[G_{2n,0,0}(0)/S(0)]$.

[b] Calculated from MD simulations by means of the virial theorem, Eq. (15).

of the a_{2n} coefficients in Eq. (12) are in satisfactory agreement with the values obtained by means of the virial theorem (see Table III). Note that calculation of the pressure in center-to-center dependent coordinates requires the angle-dependent distance of contact, and this method is consequently much less convenient.

Collision rate

We have used our data to evaluate the collision rate Z as well as the contact average $\overline{D(0)}$ specified by Eqs. (10) and (16). These values can be combined with the known value of $S(0)$ to calculate $g_{\rm iso}(0)$ by means of Eq. (15). In Table II these values are compared with those obtained by extrapolating $G_{000}(s)$ to contact ($s=0$).

Single-particle orientations: Comparison with scaled particle theory

No simple analytical theory of contact orientational properties currently exists for single-component fluids of HCB's. Boublik[6] determined the pressure of pure fluids of ellipsoids and fluid mixtures by means of scaled particle theory (SPT); She *et al.*[7] calculated the contact PDF for a single HCB in a fluid of spheres, and Perera, Kusalik and Patey[10] employed the hypernetted chain and Percus–Yevick integral equation theories in the calculation of r-based structural information for pure fluids of HCB's. Strictly, the analysis of She *et al.* is inapplicable here; however, since we have seen that the $G_{220}(s)$'s are roughly the square of the $G_{200}(s)$'s, the pair correlations should be weak. This suggests that $G_{200}(s)$ might be similar for a HCB in a fluid of HCB's (which corresponds to our MD simulations) and for a HCB in a fluid of hard spheres (which corresponds to the SPT of She *et al.*). The only property for which existing SPT and simulation results can be compared are the contact values of the single Legendre functions, $G_{2n,0,0}(0)$, or alternatively, averages of the form $\overline{\cos^n\theta}$ at contact. Figure 4 shows the SPT predictions for $\overline{\cos^2\theta_1}$ at contact for a single ellipsoid in a bath of spheres having the same volume as the ellipsoids. The SPT values decay more rapidly with density than do the MD results. Both SPT and MD results agree in one important regard: as the density increases there is an increased tendency for the solvent molecules to align on the flat portions of the convex surface.

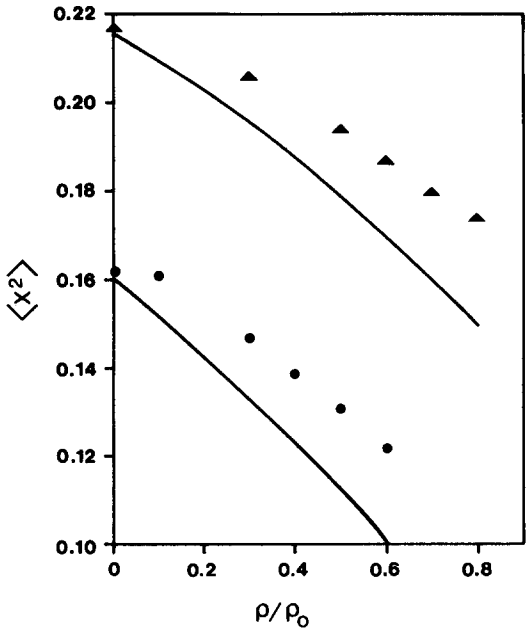

FIG. 4. Contact orientational averages of $\cos^2\theta = x^2$ from scaled particle theory (solid line) and simulation (▲ for $a/b=2$, ● for to $a/b=3$).

The orientational pair correlation factor, g_2

For comparative purposes we calculate g_2 in both center-to-center and apse-vector coordinates. In the former,

$$g_2 = \lim_{r\to\infty} g_2(r), \tag{25}$$

$$g_2(r) = 1 + \int_0^r f(r')dr', \tag{26}$$

$$f(r) = 4\pi\rho g_{000}(r)\,\overline{P_2(r)}\,r^2, \tag{27}$$

where

$$\overline{P_2(r)} = \frac{\int(d\hat{\mathbf{e}}_1/4\pi)\int(d\hat{\mathbf{e}}_2/4\pi)g(r,\hat{\mathbf{e}}_1,\hat{\mathbf{e}}_2)P_2(\hat{\mathbf{e}}_1\cdot\hat{\mathbf{e}}_2)}{g_{000}(r)}, \tag{28}$$

and $g_{000}(r)$ is the isotropic PDF and $P_2(\hat{\mathbf{e}}_1\cdot\hat{\mathbf{e}}_2)$ involves the relative orientations of two particles. This is the notation used by Impey, Madden, and Tildesley.[19] In our apse-vector-based system we have the analogous expressions

$$g_2 = \lim_{s\to\infty} g_2(s), \tag{29}$$

$$g_2(s) = 1 + \int_0^s \phi(s')ds' - g_v, \tag{30}$$

$$\phi(s) = 4\pi\rho g_{\rm iso}(s)\,\overline{P_2(s)}_J S(s), \tag{31}$$

where

$$\overline{P_2(s)}_J = \frac{\int(d\hat{\mathbf{e}}_1/4\pi)\int(d\hat{\mathbf{e}}_2/4\pi)[G(s,\hat{\mathbf{e}}_1,\hat{\mathbf{e}}_2) - J(s,\hat{\mathbf{e}}_1,\hat{\mathbf{e}}_2)]P_2(\hat{\mathbf{e}}_1\cdot\hat{\mathbf{e}}_2)}{G_{000}(s)}, \tag{32}$$

and g_v is given in Eq. (23). We note that $\overline{P_2(s)}_J$ differs from the average $\overline{P_2(s)}$, which is defined in Eq. (10), in that the effective distribution is G-J rather than G.

It is readily shown by using the spherical harmonic sum rule that[24]

$$P_2(\hat{\mathbf{e}}_1\cdot\hat{\mathbf{e}}_2) = \sum_{m=-2}^{2}(-1)^m C_{2m}(\hat{\mathbf{e}}_1)C_{2,-m}(\hat{\mathbf{e}}_2), \tag{33}$$

and so from Eq. (33) we find that

$$g_{\rm iso}(s)S(s)\,\overline{P_2(s)}_J = \sum_{m=-2}^{2}(-1)^m[G_{22m}(s) - J_{22m}(s)]. \quad (34)$$

$\overline{P_2(s)}$ is a measure of the relative pair orientation per molecule at separation s, whereas $\overline{P_2(s)}_J$ measures correlations above those present in an ideal gas of ellipsoids and hence is an indicator of density-dependent packing restrictions. Though the quantity $\overline{P_2(s)}$ is perhaps of more theoretical interest, it is $\phi(s)$ that directly determines the measured quantity g_2.

Previously, using a center-to-center formalism, Streett and Tildesley[15] and Impey, Madden, and Tildesley[19] found, using computer simulation, that at reasonably high density, $\overline{P_2(r)}$ for a model of CS_2 was an oscillatory function with a period of about $r\sim\sigma$ and an exponential decay length also of order σ. They found that $f(r)$ and $g_2(r)$ had about the same oscillation period but a decay length of about 4σ. From this behavior one concludes that the orientational correlation per molecule, $\overline{P_2(r)}$, is quite short ranged and only mildly oscillatory, but when weighted by $4\pi r^2 g_{\rm iso}(r)$, the number of particles at a distance r, the apparent correlation length is extended and the oscillatory nature more pronounced. It is this weighted average that enters into the expression for the measured quantity g_2. We examine these correlations in the apse-vector representation to see whether the connection between orientational correlation and g_2 can be simplified.

In Figs. 5–7 we examine $\overline{P_2(r)}$, $f(r)$, and $g_2(r)$, together with the analogous apse-vector quantities, $\overline{P_2(s)}_J$, $\phi(s)$, and $g_2(s)$ for $a/b=3$ ellipsoids at a reduced density of 0.6. $\overline{P_2(s)}$ and $\overline{P_2(s)}_J$ are very similar, but at large s, $\overline{P_2(s)}$ decays as $-s^{-2}$, whereas $\overline{P_2(s)}_J$ decays to zero rapidly from above. This small negative tail is repsonsible for the pathological behavior of the volume integral of $\overline{P_2(s)}$. The results are not definitive since it is not clear that we have gone to large enough values of s or r to determine g_2. However, $g_2(s)$ has an excluded volume contribution at $s=0$ and rises quickly, whereas $g_2(r)$ starts at one for $r=2b$ and then rises more slowly towards its asymptotic value. Thus, the merit of the apse-vector language is that simple excluded volume contributions are treated easily in g_v, while the long-range orientational order is represented by the $G-J$ terms. In the $g_2(r)$ representation both of these effects are mixed. It also appears that for a given value of s, $g_2(s)$ is considerably closer to its asymptotic g_2 value than is $g_2(r)$ at the corresponding value of $r-\sigma$.

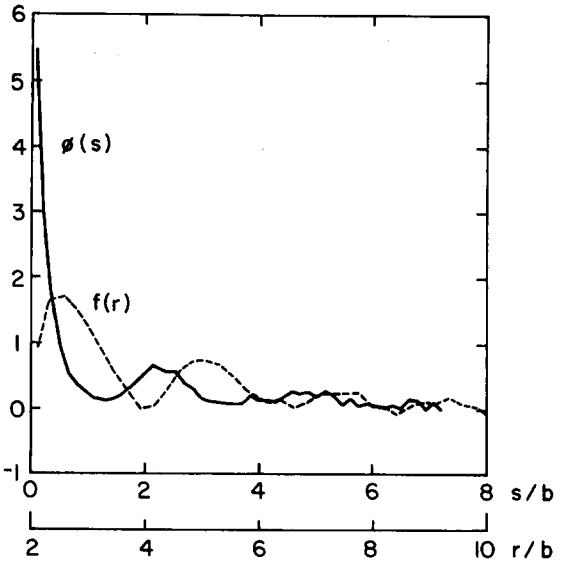

FIG. 6. Integrand for g_2 for the same fluid as in Fig. 5. The dashed line corresponds to $f(r)/4\pi\rho$ and the solid line to $\phi(s)/4\pi\rho$.

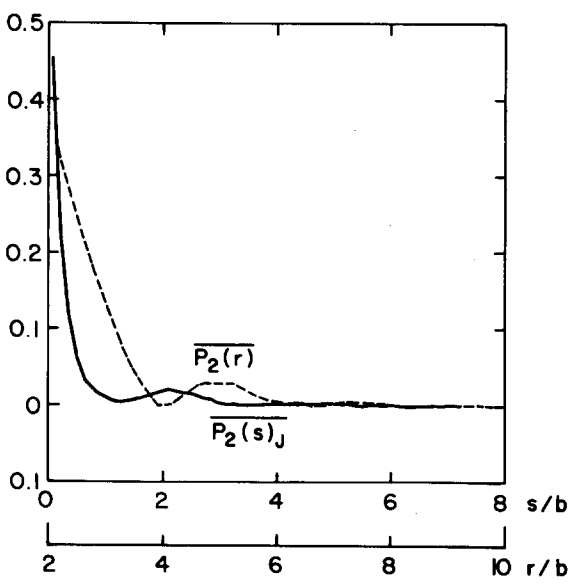

FIG. 5. Orientational correlation functions for a fluid of hard ellispoids with $a/b=3$, $\rho/\rho_0=0.6$, and $N=512$. The dashed line corresponds to $P_2(r)$ and the solid line to $P_2(s)_J$.

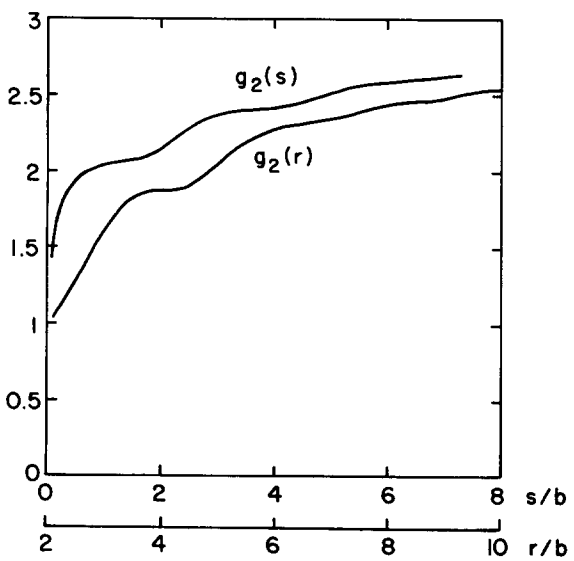

FIG. 7. $g_2(s)$ and $g_2(r)$ for the same fluid as in Fig. 5.

SUMMARY

The primary function of the MD results presented here is to evaluate the possible benefits of a HCB reference system as a basis for theories of polyatomic fluids. Since all the intermolecular forces in the HCB model are transmitted perpendicularly to the surface, the natural coordinates are derived from the surface normal (or apse vector) and the shortest surface-to-surface separation. Conventionally, center-to-center distances (plus orientations) have been employed to express intermolecular properties of atomic fluids; however, that coordinate system can at best define the potential surfaces parametrically and in a complicated fashion. The disadvantage of the apse-vector scheme is its difficulty of implementation. But given that, then what are its benefits? Contact properties such as the collision rate and the pressure are determined much more efficiently in the s language. Likewise, the isotropic PDF, $g_{\rm iso}(s)$, is simpler to interpret in this language. For example, the fact that the ellipsoids pack side by side is easily seen from the location of the second peak in $g_2(s)$. In apse-vector coordinates it can be seen that $g_2(s)$ has an appreciable surface contact contribution. See Eq. (21). We also expect that the ensemble averages of other distance-dependent functions (which vanish by symmetry at large r in the center-to-center coordinate system) will also have appreciable surface contact contributions which can be readily identified in apse coordinates.

Our work does not indicate a great advantage of the s-based over the r-based representation. Nonetheless, the result of the g_2 analysis is the unambiguous separation of g_2 into two pieces: a short-range excluded volume contribution, and an s-dependent long-range term. This result in itself might be a useful guide for future theoretical work.

ACKNOWLEDGMENTS

We would like to thank Dr. Gilles Tarjus for his very useful comments, and Professor David Hoffman for suggesting the decompostion of g_2 used in Eq. (21). This work was supported by grants from the U.S. National Science Foundation, the U.K. Science and Engineering Council, and by the Petroleum Research Foundation. Computational services were provided by the John von Neumann Center for Scientific Computing in Princeton. International travel was made possible by a travel award from NATO. The work of the FOM Institute in part of the research program of FOM and is supported by the "Nederlandse Organistie voor Wetenschappelijk Onderzoek" (NWO).

APPENDIX A

The properties of hard convex bodies (HCB's) necessary for our analysis are summarized by Kihara[5] and elsewhere.[7(a)] We review some of these properties here. One definition of a convex body is that each point on its surface has a unique surface normal, $\hat{\mathbf{s}}$. Figure 1 shows our coordinate system for a pair of convex bodies separated by a surface-to-surface distance s measured along $\hat{\mathbf{s}}$, The mathematical properties of HCB's are easily demonstrated by means of a support function, $h(x_1)$, which is defined as the projection

$$h(x_1) = \hat{\mathbf{s}}\cdot\boldsymbol{\xi}_1, \tag{A1}$$

where $\boldsymbol{\xi}_1$ is the vector extending from the center of the body to the point on the surface

$$\boldsymbol{\xi}_1 = \hat{\mathbf{s}}h(x_1) + (\mathbf{1} + \hat{\mathbf{s}}\hat{\mathbf{s}})\cdot\hat{\mathbf{e}}_1 h'(x_1). \tag{A2}$$

x_1 is $\cos\theta_1$ defined in Eq. (2) and $h'(x_1) = dh(x_1)/dx_1$. The support function for convex surface comprised of two convex bodies separated by surface-to-surface separation distance s is $\mathbf{s}\cdot\mathbf{r}(s)$, where

$$\mathbf{r}(\hat{\mathbf{s}}) = \mathbf{s} + \boldsymbol{\xi}_1(\hat{\mathbf{s}}) - \boldsymbol{\xi}_2(-\mathbf{s}). \tag{A3}$$

Given the radial vector $\mathbf{r}$ the accompanying differential element of surface area for the combined convex body is $ds\,J$,

$$d\mathbf{r} = d\theta\,d\phi\,ds\left|\hat{\mathbf{s}}\cdot(\partial\mathbf{r}/\partial\theta)\times(\partial\mathbf{r}/\partial\phi)\right| = ds\,J(s,x_1,x_2,\alpha). \tag{A4}$$

Here θ and ϕ are the polar and azimuthal angles of the apse vector $\hat{\mathbf{s}}$ with respect to the laboratory frame. After some algebra, one can show that the Jacobian is

$$J(s,x_1,x_2,\alpha) = j(j + f_1 + f_2) + f_1 f_2 \sin^2(\alpha), \tag{A5}$$

with

$$j = s + h(x_1) - x_1 h'(x_1) + h(x_2) - x_2 h'(x_2), \tag{A6a}$$

$$f_i = h''(x_i)(1 - x_i^2). \tag{A6b}$$

The properties sketched above pertain to general convex bodies. For the special case of an ellipsoid with semimajor axis a and semiminor axis b, the support function is

$$h(x) = b\sqrt{1 + \epsilon x^2} \tag{A7}$$

with $\epsilon = (a/b)^2 - 1$.

The surface function $S(s)$ for HCB's can be obtained from Eqs. (7) and (A4)–(A7):

$$S(s) = S_c/2\pi + 2R_c^2 + 4R_c s + s^2, \tag{A8}$$

where S_c is the surface area of the convex body and R_c is its mean radius of curvature. For a prolate ellipsoid,

$$S_c = 2\pi b^2\left(1 + \frac{\sin^{-1}\gamma}{\gamma\sqrt{1-\gamma^2}}\right) \tag{A9}$$

and

$$R_c = \frac{a}{2}\left(1 + \frac{1-\gamma^2}{2\gamma}\log\frac{1+\gamma}{1-\gamma}\right), \tag{A10}$$

where $\gamma^2 = (a^2 - b^2)/a^2$.

We now give analytic expressions for the first three coefficients defined by Eq. (14). Let

$$I_n = \int_0^1 dx\, x^n\sqrt{1 + \epsilon x^2}, \tag{A11}$$

then

$$2I_0 = \epsilon_1 + (1\sqrt{\epsilon})\log(\sqrt{\epsilon} + \epsilon_1), \tag{A12a}$$

$$8I_2 = \epsilon_1/\epsilon + 2\epsilon_1 - \epsilon^{-3/2}\log(\sqrt{\epsilon} + \epsilon_1), \tag{A12b}$$

$$16I_4 = \tfrac{8}{3}\epsilon_1/\epsilon - 2\epsilon_1^3/\epsilon^2 + \epsilon^{-5/2}\log(\sqrt{\epsilon} + \epsilon_1), \tag{A12c}$$

with $\epsilon_1 = \sqrt{1+\epsilon}$ and

$$a_0 = I_0, \tag{A13a}$$

$$a_2 = \tfrac{1}{2}\sqrt{5}(3I_2 - I_0), \tag{A13b}$$

$$a_4 = \tfrac{3}{8}(35I_4 - 30I_2 + 3I_0). \tag{A13c}$$

APPENDIX B

Here we evaluate g_v the integral of $P_2(\hat{\mathbf{e}}_1\cdot\hat{\mathbf{e}}_2)$ over the overlap region defined in Eq. (21) by means of a scaling argument. Define a family of convex surfaces,

$$\mathbf{r} = \lambda \mathbf{r}_0(\hat{\mathbf{s}}), \tag{B1}$$

which are λ-scaled versions of the excluded volume surface, $\mathbf{r}_0(\mathbf{s})$. If we transform the spherical volume element $d\mathbf{r}$ in the overlapping region to the family of convex surfaces with coordinates λ and s, the Jacobian is

$$d\mathbf{r} = |(\partial\mathbf{r}/\partial\theta)\times(\partial\mathbf{r}/\partial\phi)\cdot(\partial\mathbf{r}/\partial\lambda)|d\theta\, d\phi\, d\lambda. \tag{B2}$$

Application of Eq. (B1) to (B2) results in

$$d\mathbf{r} = |(\partial\mathbf{r}_0/\partial\theta)\times(\partial\mathbf{r}_0/\partial\phi)\cdot\mathbf{r}_0|d\theta\, d\phi\, d\lambda, \tag{B3}$$

and since $(\partial\mathbf{r}_0/\partial\theta)\times(\partial\mathbf{r}_0/\partial\phi)$ points along $\mathbf{s}$, it follows that

$$d\mathbf{r} = \lambda^2 h_{12} J(s=0,\hat{\mathbf{e}}_1,\hat{\mathbf{e}}_2) d\hat{\mathbf{s}}\, d\lambda \tag{B4}$$

with $h_{12} = h(x_1) + h(x_2)$. Finally, by performing the (zero to one) integral over the scaling coordinate, we find that Eq. (23) for g_v becomes Eq. (24).

APPENDIX C

In actual light scattering experiments one measures $g_2(\mathbf{q})$ where

$$g_2 - 1 = \rho \int d\mathbf{r} \int (d\hat{\mathbf{e}}_1/4\pi) \int (d\hat{\mathbf{e}}_2/4\pi) \times P_2(\hat{\mathbf{e}}_1\cdot\hat{\mathbf{e}}_2) g(r,\hat{\mathbf{e}}_1,\hat{\mathbf{e}}_2) e^{i\mathbf{q}\cdot\mathbf{r}}. \tag{C1}$$

For $q = 0$, this equation reduced to Eq. (19). Though one is often interested in very small q, i.e., $q\to 0$, one is always interested in finite q, i.e., $q\neq 0$. Equation (C1) can be rewritten as

$$g_2 - 1 = \rho \int d\mathbf{r} \int \left(\frac{d\hat{\mathbf{e}}_1}{4\pi}\right) \times \int \left(\frac{d\hat{\mathbf{e}}_2}{4\pi}\right) P_2(\hat{\mathbf{e}}_1\cdot\hat{\mathbf{e}}_2)[g(r,\hat{\mathbf{e}}_1,\hat{\mathbf{e}}_2) - 1]e^{i\mathbf{q}\cdot\mathbf{r}} + \rho\delta(\mathbf{q}) \times \int \left(\frac{d\hat{\mathbf{e}}_1}{4\pi}\right) \int \left(\frac{d\hat{\mathbf{e}}_2}{4\pi}\right) P_2(\hat{\mathbf{e}}_1\cdot\hat{\mathbf{e}}_2). \tag{C2}$$

The integrand in the first term converges sufficiently rapidly with increasing r, that for small q we can set $q = 0$. In the second term we observe the conditional convergence mentioned in the text: if $q\neq 0$, the convergence is absolute, but if $q = 0$ the term is indeterminate. So provided we exclude $q = 0$, which is an actual experimental requirement, we can neglect the second term in Eq. (C2). (One can envisage L as the length of the container, and so we require that $qL > 1$; in the thermodynamic limit, $L\to\infty$, and we can let $q\to 0$, but subject to the condition $qL > 0$.) The first term in Eq. (C2) can be rewritten as in Eq. (20), and therefore one obtains Eq. (21).

[1] E.g., J.-P. Hansen and I. R. McDonald, *Theory of Simple Liquids*, 2nd ed. (Academic, New York, 1986).
[2] J. A. Barker and D. Henderson, Rev. Mod. Phys. **48**, 587 (1976).
[3] D. Chandler, in *The Liquid State of Matter: Fluids, Simple and Complex*, edited by E. W. Montroll and J. L. Lebowitz (North-Holland, Amsterdam, 1982).
[4] C. G. Gray and K. E. Gubbins, *Theory of Molecular Liquids 1. Fundamentals* (Clarendon, Oxford, 1984).
[5] T. Kihara, Adv. Chem. Phys. **5**, 147 (1963).
[6] T. Boublik, Mol. Phys. **51**, 1429 (1984).
[7] (a) R. S. C. She and G. T. Evans, J. Chem. Phys. **85**, 1513 (1986); (b) R. S. C. She, C. James, and G. T. Evans, J. Chem. Phys. **85**, 1525 (1986).
[8] R. G. Cole and G. T. Evans, Annu. Rev. Phys. Chem. **37**, 105 (1986).
[9] D. Frenkel, Mol. Phys. **60**, 1 (1987).
[10] A. Perera, P. G. Kusalik, and G. N. Patey, J. Chem. Phys. **87**, 1295 (1987); Mol Phys. **60**, 77 (1987).
[11] W. A. Steele, J. Chem. Phys. **39**, 3197 (1963).
[12] L. Blum, J. Chem. Phys. **57**, 1862 (1972); **58**, 3295 (1973).
[13] W. B. Streett and D. J. Tildesley, Proc. R. Soc. London Ser. A **355**, 239 (1977).
[14] V. N. Kabadi and W. A. Steele, Ber. Bunsenges. Phys. Chem. **89**, 9 (1985).
[15] B. Kumar, C. James, and G. T. Evans, J. Chem. Phys. **88**, 7071 (1988).
[16] F. Ghazi and M. Rigby, Mol. Phys. **62**, 1103 (1987).
[17] D. W. Rebertus and K. M. Sando, J. Chem. Phys. **67**, 2585 (1977).
[18] T. Keyes and D. Kivelson, J. Chem. Phys. **56**, 1057 (1972).
[19] R. W. Impey, P. A. Madden, and D. J. Tildesley, Mol. Phys. **44**, 1319 (1981).
[20] D. J. Adams, Chem. Phys. Lett. **62**, 329 (1979).
[21] M. P. Allen, D. Frenkel, and J. Talbot, Comput. Phys. Rep. **9**, 301 (1989).
[22] M. S. Wertheim and J. Talbot (unpublished).
[23] G. J. Throop and R. J. Bearman, J. Chem. Phys. **42**, 2408 (1965); L. Verlet and J. -J. Weis, Phys. Rev. A **5**, 939 (1972).
[24] E.g., D. M. Brink and G. R. Satchler, *Angular Momentum* (Oxford, New York, 1968).